A Method for Subject Specific Estimation of Aortic Wall Shear Stress

Johan Renner
Applied Thermodynamics and Fluid Mechanics
Department of Management and Engineering
Linköping University, 581 83 Linköping
SWEDEN
Johan.Renner@liu.se

Roland Gårdhagen
Applied Thermodynamics and Fluid Mechanics
Department of Management and Engineering
Linköping University
SWEDEN

Tino Ebbers
Department of Medical and
Health Sciences/Clinical Physiology
Linköping University
SWEDEN

Einar Heiberg
Department of Clinical Physiology
Lund University Hospital
SWEDEN

Toste Länne
Department of Medical and
Health Sciences/Clinical Physiology
Linköping University
SWEDEN

Matts Karlsson
Applied Thermodynamics and Fluid Mechanics
Department of Management and Engineering
Linköping University
SWEDEN

Abstract: Wall shear stress (WSS) distribution in the human aorta is a highly interesting hemodynamic factor for atherosclerosis development. We present a magnetic resonance imaging (MRI) and computational fluid dynamics (CFD) based subject specific WSS estimation method and demonstrate it on a group of nine healthy volunteers (males age 23.6 ± 1.3 years). In all nine subjects, the aortic blood flow was simulated in a subject specific way, where the 3D segmented geometries and inflow profiles were obtained using MRI. No parameter settings were tailored using data from the nine subjects. Validation was performed by comparing CFD gained velocity with magnetic resonance imaging (MRI) velocity measurements.
CFD and MRI velocity profiles were comparable, but the temporal variations of the differences during the cardiac cycle were significant. Spatio-temporal analyzes on the WSS distribution showed a strong subject specific influence. Subject specific models are decisive to estimate WSS distribution.

Key–Words: WSS, Aorta, Subject Specific, MRI, CFD, Velocity Validation, 3D segmentation

1 Introduction

Cardiovascular disease originating from atherosclerosis is the number one killer in Western world (1). Several risk factors are associated with the development of atherosclerosis e.g. smoking, lack of physical activity, and plasma lipid levels (2; 3; 4; 5; 6). Local hemodynamic factors may also be of importance as the localization of atherosclerosis is highly non-uniform (7; 2). Recent studies also show a possible relationship between certain hemodynamic parameters and intima-media thickness (a known atherosclerosis indicator) for the carotid arteries (8) as well as for the coronary arteries (6).

By combining recent development in in-vivo imaging, image processing and numerical methods, subject specific wall shear stress (WSS) can be estimated using magnetic resonance imaging (MRI) and computational fluid dynamics (CFD). Prior studies have used MRI combined with CFD to predict flow and WSS in subject specific human arteries e.g. (9; 10; 11; 12; 13) and all these studies emphasize the importance of using a subject specific approach. However, the small number of subjects (generally one) in these studies does not show the full potential of the subject specific approach. Furthermore CFD simulations always require validation of the result, which is especially challenging in the case of a very complex geometry such as subject specific human artery. Recent reviews (14; 15) request development of subject specific methods, in-vivo velocity

validation and clinical relevant methods. We have previously reported the feasibility of our approach for WSS estimation using MRI and CFD (16).

The goal with this work is to: 1) present an approach (method) for subject specific in-vivo WSS estimations suitable for the clinical setting, 2) validate the CFD velocity result using MRI velocity measurement and 3) apply the WSS estimation method to a group of nine healthy volunteers (age 21-26).

2 Method

Geometrical as well as flow data were acquired using a 1.5 T MRI scanner (Philips Achieva, Philips Medical Systems, Best, The Netherlands). Geometrical information of the complete aorta was obtained within a breath hold using a 3D gadolinium-enhanced gradient-echo sequence (echo time 1.6 ms, repetition time 5.3 ms, and flip angle 40°, field of view 400x360x80 mm^3, acquisition matrix 400x230x80, SENSE factor 1.5). A 30 ml (0.5 mmol/ml) contrast bolus (Omniscan, Amersham Health, Oslo, Norway) was injected at 2.0 ml/s. Randomly segmented central k-space ordering (CENTRA) was used. The 3D volume data was reconstructed to a resolution of 0.78x0.78x1.00 mm^3.

Time-resolved aortic flow velocities were obtained by performing a through-plane 2D velocity MRI acquisition (echo time 2.3 or 2.4 ms, repetition time 3.9 or 4.0 ms, flip angle 15, velocity encoding range 1.5 or 2.0 m/s) placed supracoronary perpendicular to the flow direction. The acquisition was performed during a breath hold using SENSE factor 2.0 and retrospective cardiac gating to a vectorcardiogram. A 10 mm thick slice was acquired with a field of view of 350x297 mm^2, acquisition matrix 144x122. The acquired data were reconstructed to 40 time-frames per cardiac cycle with a spatial resolution of 1.37x1.37 mm^2. The velocity data were corrected for the effects of concomitant gradient fields and eddy currents on the scanner.

A 3D level set algorithm was used for segmentation. In the image-volume one or several seed points/regions are defined and an implicit surface is allowed to expand out-wards to the edge of the object (17). An edge image I_{edge} was calculated as:

$$I_{edge} = \sqrt{(I * f_x)^2 + (I * f_y)^2 + (I * f_z)^2} \quad (1)$$

where I is the normalized image volume, f_i is the derivative filter kernel using central difference approximation, and $*$ denotes 3D convolution.

The expansion speed is determined by a speed image and the local curvature. The speed image was calculated as:

$$I_{speed} = f(x) - I_{edge}; \qquad x = 16(I - i_{obj} - I_{offset})$$

$$f(x) = \begin{cases} 2 & x \geq 2 \\ 0 & -2 < x < 2 \\ -2 & x \leq -2 \end{cases}$$

$$(2)$$

where i_{obj} is the mean intensity in the seed points. The parameter I_{offset} was set to 0.15 by the software operator. The local expansion speed V_{exp}, was calculated as:

$$V_{exp} = I_{speed} - \beta\kappa \quad (3)$$

where κ is a local curvature estimate, and β is a coefficient determining the importance of the local curvature. To improve segmentation a rough curvature estimate was used (18), which improves the segmentation speed several magnitudes compared to traditional level set algorithms.

The binary output from the level set was smoothed using a 3D Gaussian smoothing filter with a smoothing radius of 2 mm. The spatial size of the filter was 19 pixels. The smoothed level set object was converted to a surface description using a marching cubes algorithm (19).

The total time for the segmentation was approximately 20 minutes per subject (a manual approach would take 16 h per subject). The algorithm was implemented into a cardiac image analysis software package (20).

The surface description was used to create a mesh using tetrahedral cells using ICEM 10.0 (ANSYS, Inc., Canonsburg, Pennsylvania, USA). The meshes consisted of 1.5-2.5 Mcells, the size of the meshes were determined by conducting mesh indepentent studies. CFD simulations were performed using Ansys Fluent 6.1.18 (Ansys Inc., Pittsburgh, Pennsylvania, USA). The inlet at the ascending aorta was treated as a time dependent velocity inlet where a subject specific velocity profile from MRI was used. The measured velocity profile (perpendicular to the cross-section) was linearly interpolated to fit the apropriate simulation time-step (0.01 s).

The brachiocephalic, left common carotid and
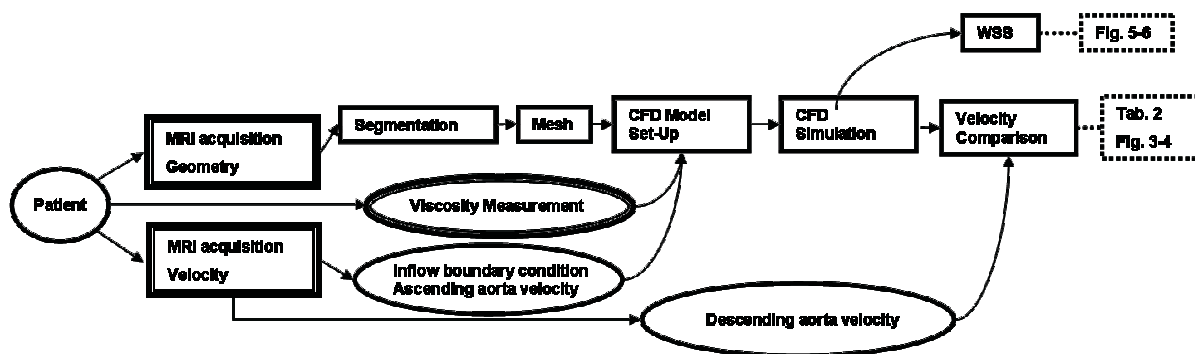
Figure 1: The work-flow conducted describing the WSS estimating method and the velocity comparison strategy.

Table 1: Weight, length, BMI and blood viscosity in the nine subjects.

Subject	Weight [kg]	Length [m]	BMI [kg/m^2]	Viscosity [kg/ms]
1	68	1.79	21.2	0.0043
2	77	1.84	22.7	0.0062
3	69	1.81	21.1	0.0039
4	67	1.82	20.2	0.0045
5	73	1.86	21.1	0.0046
6	72	1.87	20.6	0.0046
7	71	1.78	22.4	0.0055
8	83	1.84	24.5	0.0037
9	75	1.79	23.4	0.0041
	73±5	1.82±0.03	21.9±1.3	0.0046±0.0007

left subclavian artery on the aortic arch were treated as mass-flow outlets with a fixed mass-flow fraction. The outflow in the thoracic aorta was set to 80 %. In subjects with three aortic arch outflows the fractions were set to 10-5-5 % and in the subject with two outflows the fractions were fixed to 10-10 %. The aortic wall was treated as a rigid wall with a no slip boundary condition. The flow was assumed to be laminar and Re_{inlet} based on cross-section mean velocity were in the range 0-3000 during the whole cardiac cycle. The blood was assumed to be Newtonian with a constant subject specific viscosity (Table 1), and the density was set to 1060 kg/m^3 (21). The Navier-Stokes equations:

$$\nabla \cdot \mathbf{u} = 0 \qquad (4)$$

$$\rho\left(\frac{\partial \mathbf{u}}{\partial t} + (\mathbf{u} \cdot \nabla)\mathbf{u}\right) = -\nabla p + \mu\nabla^2\mathbf{u} \qquad (5)$$

were solved in the flow domain, where $\mathbf{u}$ is velocity, p pressure, ρ density and μ the dynamic viscosity.

Along two perpendicular axes, anterior-posterior (A-P) and left-right (L-R) in the descending aorta, CFD and MRI velocity profiles (V_{CFD}, V_{MRI})

were compared (Figure 2). In order to evaluate the similarity between the two velocity profiles, differences between the profiles were calculated after normalizing by the maximum velocity described by:

$$\Delta_i = \frac{V_{CFD,i}}{max(V_{CFD,i})} - \frac{V_{MRI,i}}{max(V_{MRI,i})} \quad \forall i \quad (6)$$

where i indicates moving along the A-P and L-R axis. V_{CFD} was linearly resampled to a coarser resolution to fit V_{MRI} (Figure 3). The normalized differences, Δ_i, were condensed into a root mean square (RMS) value:

$$\mathrm{RMS} = \sqrt{\frac{\sum_i \Delta_i^2}{n_i}} \qquad (7)$$

A Linux cluster at National Supercomputer Center (NSC), Linköping University, Sweden, was used as a computational resource for the CFD simulations.

3 Material

Nine healthy male volunteers (23.6 ± 1.3 years) participated in the study. They were all non smokers, with normal blood pressure levels (<140/90 mm Hg)
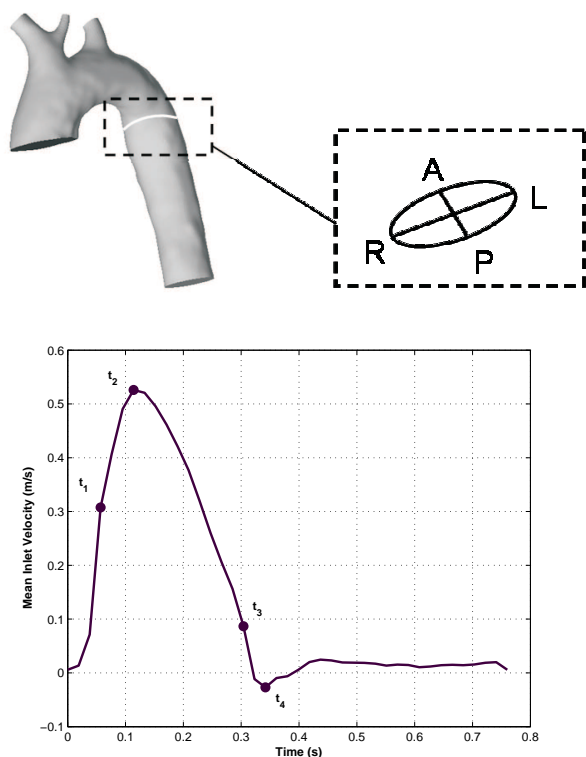
Figure 2: *Top:* A geometrical model of the aortic arch (subject #3) with the velocity comparison location marked and the directions anterior (A), posterior (P), left (L) and right (R) schematically indicated. *Bottom:* Mean velocity at the inlet (subject 3) with the time points marked, defined as maximum acceleration (t_1), maximum velocity (t_2), maximum retardation (t_3) and minimum velocity (t_4).

Figure 3: Velocity profiles in the thoracic ascending aorta for subject #3, MRI measured velocity profiles (circles) and CFD simulated profiles (solid line) at both anterior-posterior (A-P) and left-right (L-R) directions.
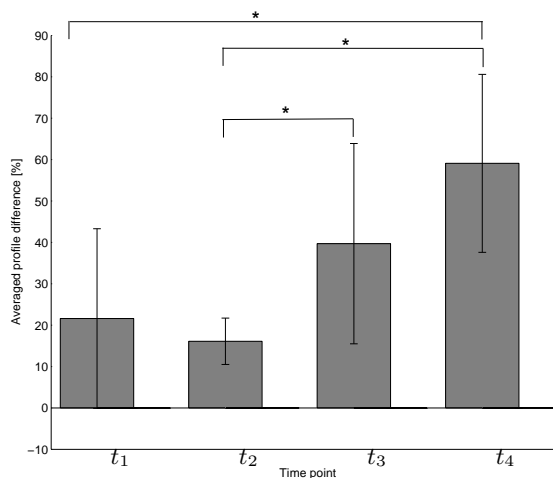
Figure 4: Subject and direction (A-P and L-R) mean values and standard deviation of the velocity profile difference RMS values for the four different time positions $t_1 - t_4$. Values describes the velocity profile difference with respect to the maximum amplitude of the velocity profiles. A-P and L-R directions gave same profile form differences see Table 2. * significant at level $p < 0.05$

and without a history of cardiovascular disease. The volunteers where not taking any medication. The average weight was 73 ± 5 kg and the average body mass index was 21.9 ± 1.3 kg/m^2. Average dynamic blood viscosity was 0.0046 ± 0.0007 kg/m s measured with a ReoRox$^®$ Jr. device (MediRox AB, Nyköping, Sweden) for each subject (Table 1). All volunteers gave informed consent, and the study was approved by the regional Ethics Committee for Human Research at Linköping University, Sweden.

4 Results

A method is developed for subject specific in-vivo WSS estimation which have the ability to be used in the clinical setting. No parameter settings were tailored using data from the nine subjects.

In order to evaluate the method two perpendicu-

lar velocity profiles were studied. V_{CFD} and V_{MRI} were compared for all nine subjects at four different times in the cardiac cycle. These times were based on the inlet mean velocity: maximum acceleration

Table 2: The velocity profile difference as a RMS value (%) at anterior - posterior and left-right axes in the descending aorta.

Anterior-Posterior

Subject\ Time	t_1	t_2	t_3	t_4	Mean±sd
1	12	38	40	18	27±14
2	75	11	55	46	47±26
3	29	14	10	44	24±15
4	7	9	8	48	18±20
5	20	19	32	83	38±30
6	22	8	8	87	31±38
7	4	15	98	98	54±51
8	20	18	36	38	28±11
9	12	13	78	78	45±38
Mean±sd	22±21	16±9	40±32	60±27	

Left-Right

Subject\ Time	t_1	t_2	t_3	t_4	Mean±sd
1	13	7	33	54	27±21
2	79	12	20	37	37±30
3	15	5	10	47	19±19
4	11	29	45	34	30±14
5	9	31	38	80	39±30
6	23	8	16	86	33±36
7	5	21	52	80	39±33
8	21	14	55	55	36±22
9	12	18	81	51	40±32
Mean±sd	21±23	16±9	38±22	58±19	

(t_1), maximum velocity (t_2), maximum retardation (t_3) and minimum velocity (t_4), illustrated in Figure 2. By comparing the shape of the flow profile (Figure 3) for all subjects at all times (t_1, t_2, t_3 and t_4), the difference between CFD simulated and MRI measured profiles was dependent on subject as well as time (Table 2). Subject mean values of velocity profile RMS difference for A-P and L-R were not significantly different. The RMS data are presented as a velocity profile difference of the two directions combined in Figure 4.

The 3D WSS distribution from the CFD simulations was obtained over the whole cardiac cycle for all subjects. The WSS distribution at time t_1 (maximum acceleration) is shown in Figure 5 for all nine subjects. Figure 6 shows a spatio-temporal map of the WSS magnitude distribution with circumferential position vs. time for all subjects. When analyzing all individual WSS maps there were significant subject specific detail differences in the WSS distribution.

5 Discussion

We estimated subject specific WSS in the aorta of nine healthy volunteers. Our protocol has the ability to be used in a clinical setting. This is achieved by the short MRI acquisition time and the use of semiautomatic segmentation, which takes about 20 minutes compared to about 16 hours (based on former experience) for a manual segmentation procedure. Further, the CFD simulations are easily performed in the time window over night when using a Linux cluster capacity.

In contrast to earlier studies, generally with one subject, we have investigated a group of nine subjects. In this study we include ascending aorta, the aortic arch (brachiocephalic, left common carotid and left subclavian artery included) and the descending aorta. Previous studies including comparisons between measured and CFD simulated velocities (12; 13; 9) are all hampered by the small amount of subjects used (generally one). This limits the possibility to generalize the findings.
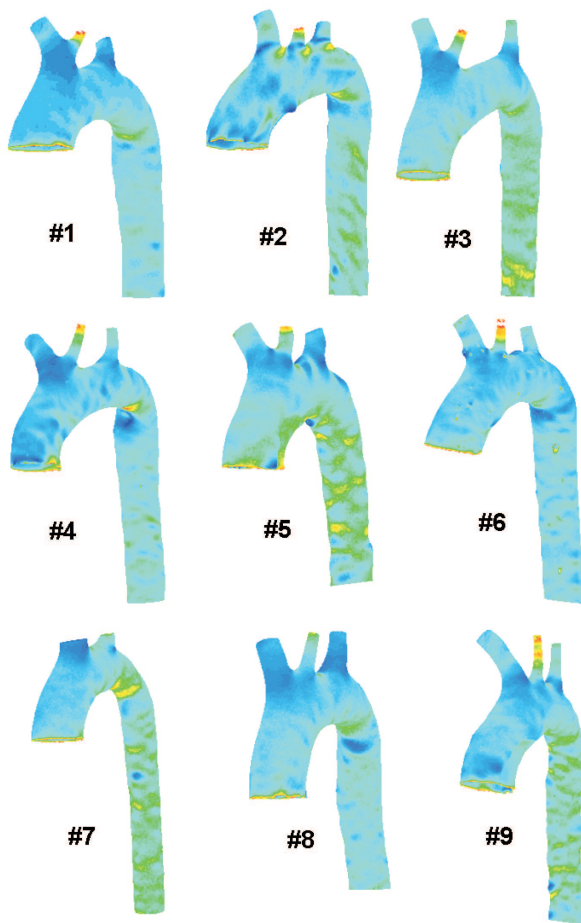
Figure 5: WSS magnitude distribution on the aortic arch for all nine subjects at time point t_1 (maximum acceleration).

In the MRI setting we acquired all necessary data in two breath hold acquisitions. The short acquisition time allows the method to be a part of a standard clinical investigation. Furthermore a direct 3D segmentation method was used to capture the geometrical complexity of arteries. Prior studies e.g. (9; 10; 11) mainly use a 2D slice segmentation approach, where a set of 2D segments is combined into a 3D geometry instead of a direct 3D approach, which has only been used in a few studies (22; 23). The importance of this aspect in getting a correct arterial geometry is also discussed by Steinman (24).

Comparing CFD and MRI velocity profiles showed a large influence of subject as well as time. Generally the relation was $V_{CFD} > V_{MRI}$ at t_1 (maximum acceleration) and t_2 (maximum velocity), $V_{CFD} \simeq V_{MRI}$ at t_3 (maximum retardation) and $V_{CFD} < V_{MRI}$ at t_4 (minimum velocity); exemplified by subject 3 in Figure 3.

The difference between simulated and measured velocity profiles is generally quite small (Figure 3), however, the RMS values show a somewhat larger difference (Table 2). The RMS values (Table 2) showed that the differences (between velocity profile form) were similar comparing the anterior-posterior and the left-right results. In Figure 4 it can be noted that the spread in RMS values were smaller at the maximum velocity time (t_1) then in the other parts of the cardiac cycle.

The larger differences at the maximum retardation and minimum velocity temporal positions can be caused by the use of rigid walls in the CFD model and the pulse wave reflection effect. In the human aorta the compliance results in a so called windkessel effect that reduces the temporal variations especially noted in the diastolic part of the cardiac cycle. This was also noted in a study (11) regarding the ascending aorta.

WSS distribution in the spatio-temporal maps in Figure 6 shows the need of subject specific estimations of WSS due to the spatial differences between the subjects. The temporal differences are also prominent, so any kind of temporal mean should be handled with care.

The use of fixed outflow fractions in the models will influence the CFD velocity profile. In reality, these fractions have probably both subject and temporal variations. Differences can also originate from the fact that the measured velocities were averaged in a 10 mm thick disk. In the CFD modeling the aortic wall was considered rigid, which results in more rapid flow changes compared with a more distensible wall (25). The use of a Newtonian model is valid since the shear rates seldom reach values where non-Newtonian effects are prominent. The assumption of laminar flow is valid for the aortic blood flow in healthy subjects since the critical Reynolds number is higher in pulsating flow than in steady state flow (7). The Reynolds number during the pulses seldom exceeds the critical steady state Reynolds number.

In conclusion, subject specific models are decisive to estimate WSS distribution. The use of spatio-temporal map of WSS enables a simple and intuitive display of the WSS distribution in a circumferential cross-section over time. When combined with the WSS distribution of the entire domain it is well suited for applications in the clinical setting, even on a routinely basis.
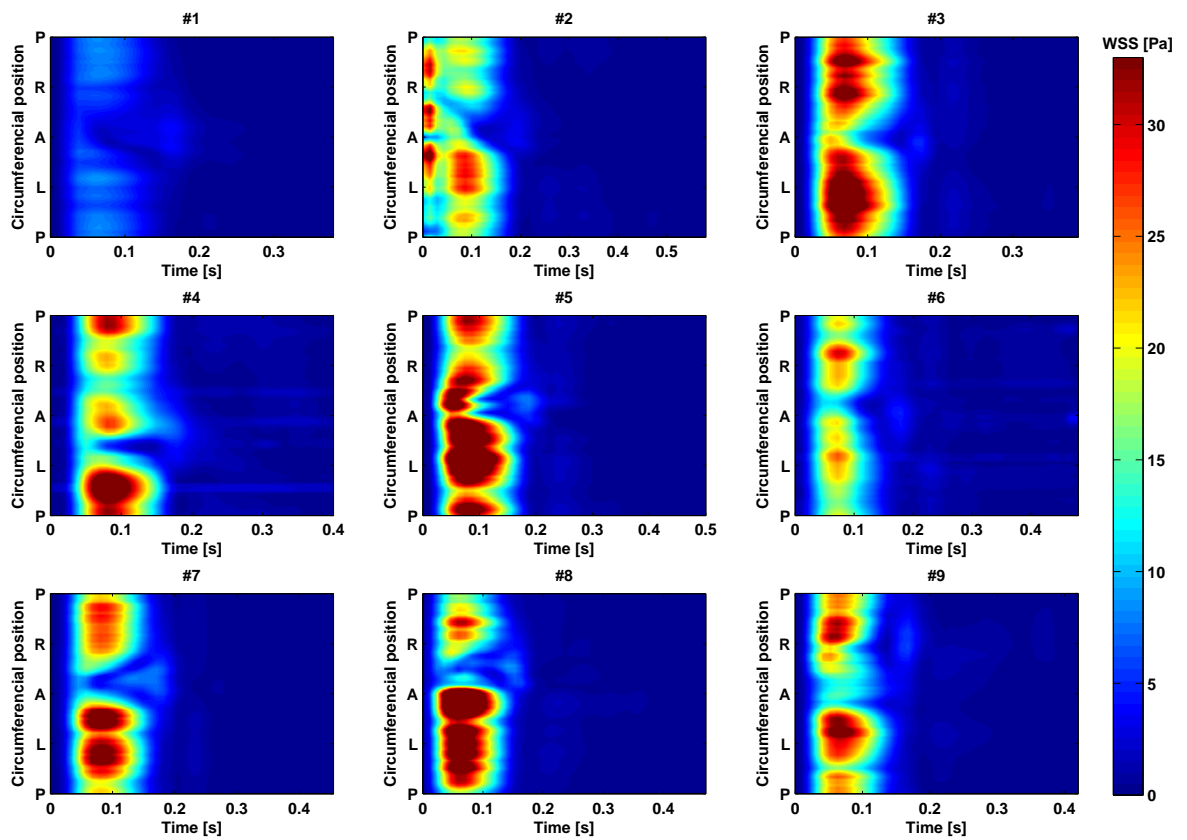
Figure 6: Spatio temporal maps of WSS magnitude for all nine subjects. In a cross-section at the ascending aorta with positions marked as: anterior (A), posterior (P), left (L) and right (R).

References:

[1] R. Ross, The pathogenesis of atherosclerosis: a perspective for the 1990s, Nature 362 (6423) (1993) 801–809.

[2] J. Humprey, Cardiovascular Solid Mechanics, Springer-Verlag, 2002.

[3] G. Berenson, S. Srinivas, W. Bao, W. Newman III, R. Tracy, W. Wattingney, Association between multiple cardiovascular risk factors and atherosclerosis in childeren and young adults, The New England Journal of Medicine 338 (1998) 1650–1656.

[4] E. J. Mayer-Davis, R. J. D'Agostino, A. J. Karter, S. M. Haffner, M. J. Rewers, M. Saad, R. N. Bergman, Intensity and amount of physical activity in relation to insulin sensitivity: the Insulin Resistance Atherosclerosis Study, JAMA 279 (9) (1998) 669–674.

[5] G. Howard, L. E. Wagenknecht, G. L. Burke, A. Diez-Roux, G. W. Evans, P. McGovern, F. J. Nieto, G. S. Tell, Cigarette smoking and progression of atherosclerosis: The Atherosclerosis Risk in Communities (ARIC) Study, JAMA 279 (2) (1998) 119–124.

[6] Y. S. Chatzizisis, A. U. Coskun, M. Jonas, E. R. Edelman, C. L. Feldman, P. H. Stone, Role of endothelial shear stress in the natural history of coronary atherosclerosis and vascular remodeling: molecular, cellular, and vascular behavior, J Am Coll Cardiol 49 (25) (2007) 2379–2393.

[7] Y. C. Fung, Biomechanics, Motion, Flow, Stress, and Growth, Springer-Verlag, 1990.

[8] A. D. Augst, B. Ariff, S. A. G. McG Thom, X. Y. Xu, A. D. Hughes, Analysis of complex flow and the relationship between blood pressure, wall shear stress, and intima-media thickness in the human carotid artery, Am J Physiol Heart Circ Physiol 293 (2) (2007) 1031–1037.

[9] Q. Long, X. Y. Xu, M. Bourne, T. M. Griffith, Numerical study of blood flow in an anatomically realistic aorto-iliac bifurcation generated from MRI data, Magn Reson Med 43 (4) (2000) 565–576.

[10] A. Leuprecht, K. Perktold, S. Kozerke, P. Boesiger, Combined CFD and MRI study of blood flow in a human ascending aorta model, Biorheology 39 (2002) 425–429.

[11] J. Suo, J. Oshinski, D. P. Giddens, Effects of wall motion and compliance on flow patterns in the ascending aorta, J Biomech Eng 125 (3) (2003) 347–354.

[12] J. Suo, Investigation of blood flow patterns and hemodynamics in the human ascending aorta and major trunks of right and left coronary arteries using magnetic resonance imaging and computational fluid dynamics, Ph.D. thesis, Georgia Institute of Technology (2005).

[13] A. Leuprecht, S. Kozerke, P. Boesiger, K. Perktold, Blood flow in the human ascending aorta: a combined MRI and CFD study, Journal of Engineering Mathematics 47 (December 2003) 387–404(18).

[14] M. Friedman, D. Giddens, Blood flow in major blood vessels-modeling and experiments, Ann Biomed Eng 33 (2005) 1710–1713.

[15] D. A. Steinman, C. A. Taylor, Flow imaging and computing: large artery hemodynamics, Ann Biomed Eng 33 (12) (2005) 1704–1709.

[16] J. Renner, R. Gårdhagen, E. Heiberg, T. Ebbers, D. Loyd, T. Länne, M. Karlsson, Feasibility of patient specific aortic blood flow cfd simulation., in: Proceedings of Medical Image Computing and Computer-Assisted Intervention - MICCAI 2006 : October 2006; Copenhagen, 2006, pp. 257–263.

[17] J. A. Sethian, Level set methods and fast marching methods, Cambridge University Press, Cambridge, USA, 1999, ISBN 0 521 64557 3.

[18] B. Nilsson, A. Heyden, A fast algorithm for level set-like active contours, Pattern Recognition Letters 24 (9-10) (2003) 1331–1337.

[19] W. E. Lorensen, H. E. Cline, Marching cubes: A high resolution 3D surface construction algorithm, in: SIGGRAPH '87: Proceedings of the 14th annual conference on Computer graphics and interactive techniques, Vol. 21, ACM Press, New York, NY, USA, 1987, pp. 163–169.

[20] E. Heiberg, L. Wigström, M. Carlsson, A. Bolger, M. Karlsson, Time resolved three-dimensional automated segmentation of the left ventricle, in: Computers in Cardiology, Lyon, France, Vol. 32, 2005, pp. 599–602, http://segment.heiberg.se.

[21] S. Berger, W. Goldsmith, E. Lewis, Introduction to Bioengineering, Oxford University Press Inc., Bath, Great Britain, 1996.

[22] Y. Yang, S. George, D. Martin, A. Tannenbaum, D. Giddens, 3D Modeling of Patient-Specific Geometries of Portal Veins Using MR Images, Conf Proc IEEE Eng Med Biol Soc 1 (2006) 5290–5293.

[23] H. Ladak, J. Milner, D. Steinman, Rapid three-dimensional segmentation of the carotid bifurcation from serial MR images, J Biomech Eng 122 (2000) 96–99.

[24] D. Steinman, Image-based computational fluid dynamics modeling in realistic arterial geometries, Ann Biomed Eng 30 (2002) 483–497.

[25] T. Länne, H. Stale, H. Bengtsson, D. Gustafsson, D. Bergqvist, B. Sonesson, H. Lecerof, P. Dahl, Noninvasive measurement of diameter changes in the distal abdominal aorta in man, Ultrasound Med Biol 18 (1992) 451–457.